

# Background Light in Potential Sites for the ANTARES Undersea Neutrino Telescope

P. Amram<sup>j</sup>, S. Anvar<sup>d</sup>, E. Aslanides<sup>a</sup>, J-J. Aubert<sup>a</sup>,  
R. Azoulay<sup>d</sup>, S. Basa<sup>a</sup>, Y. Benhammou<sup>e</sup>, F. Bernard<sup>a</sup>,  
V. Bertin<sup>a</sup>, M. Billault<sup>a</sup>, P-E. Blanc<sup>a</sup>, F. Blanc<sup>c</sup>, R.W. Bland<sup>d</sup>,  
F. Blondeau<sup>d</sup>, N. Bottu<sup>d</sup>, J. Boulesteix<sup>j</sup>, B. Brooks<sup>k</sup>,  
J. Brunner<sup>a</sup>, A. Calzas<sup>a</sup>, C. Carloganu<sup>a</sup>, E. Carmona<sup>h</sup>,  
J. Carr<sup>a</sup>, P-H. Carton<sup>d</sup>, S. Cartwright<sup>ℓ</sup>, R. Cases<sup>h</sup>, F. Cassol<sup>a</sup>,  
C. Compere<sup>f</sup>, S. Cooper<sup>k</sup>, G. Coustillier<sup>c</sup>, N. de Botton<sup>d</sup>,  
P. Deck<sup>d</sup>, F.E. Desages<sup>d</sup>, J-J. Destelle<sup>a</sup>, G. Dispau<sup>d</sup>,  
J.F. Drogou<sup>f</sup>, F. Drouhin<sup>e</sup>, P-Y. Duval<sup>a</sup>, F. Feinstein<sup>d</sup>,  
D. Festy<sup>f</sup>, J. Fopma<sup>k</sup>, J-L. Fuda<sup>c</sup>, P. Goret<sup>d</sup>, L. Gosset<sup>d</sup>,  
J-F. Gournay<sup>d</sup>, J.J. Hernández<sup>h</sup>, G. Herrouin<sup>f</sup>, F. Hubaut<sup>a</sup>,  
J.R. Hubbard<sup>d</sup>, D. Huss<sup>e</sup>, M. Jaquet<sup>a</sup>, N. Jelley<sup>k</sup>, E. Kajfasz<sup>a</sup>,  
M. Karolak<sup>d</sup>, A. Kouchner<sup>d</sup>, V. Kudryavtsev<sup>ℓ</sup>, D. Lachartre<sup>d</sup>,  
H. Lafoux<sup>d</sup>, P. Lamare<sup>d</sup>, J-C. Languillat<sup>d</sup>, D. Laugier<sup>a</sup>,  
J-P. Laugier<sup>d</sup>, Y. Le Guen<sup>f</sup>, H. Le Provost<sup>d</sup>, A. Le Van Suu<sup>a</sup>,  
L. Lemoine<sup>f</sup>, P.L. Liotard<sup>a</sup>, S. Loucatos<sup>d</sup>, P. Magnier<sup>d</sup>,  
M. Marcelin<sup>j</sup>, L. Martin<sup>a</sup>, A. Massol<sup>f</sup>, B. Mazeau<sup>d</sup>,  
A. Mazure<sup>i</sup>, F. Mazéas<sup>f</sup>, J. McMillan<sup>ℓ</sup>, C. Millot<sup>c</sup>, P. Mols<sup>d</sup>,  
F. Montanet<sup>a</sup>, J.P. Morel<sup>f</sup>, L. Moscoso<sup>d</sup>, S. Navas<sup>a</sup>,  
C. Olivetto<sup>a</sup>, N. Palanque-Delabrouille<sup>d</sup>, A. Pallares<sup>e</sup>,  
P. Payre<sup>a</sup>, P. Perrin<sup>d</sup>, A. Pohl<sup>a</sup>, J. Poinsignon<sup>d</sup>, R. Potheau<sup>a</sup>,  
Y. Queinec<sup>d</sup>, C. Racca<sup>g</sup>, M. Raymond<sup>a</sup>, J.F. Rolin<sup>f</sup>,  
Y. Sacquin<sup>d</sup>, J-P. Schuller<sup>d</sup>, W. Schuster<sup>k</sup>, N. Spooner<sup>ℓ</sup>,  
T. Stolarczyk<sup>d</sup>, A. Tabary<sup>d</sup>, M. Talby<sup>a</sup>, C. Tao<sup>a</sup>, Y. Tayalati<sup>d</sup>,  
L.F. Thompson<sup>ℓ</sup>, R. Triay<sup>b</sup>, T. Tzvetanov<sup>e</sup>, P. Valdy<sup>f</sup>,  
P. Vernin<sup>d</sup>, E. Vigeolas<sup>a</sup>, D. Vignaud<sup>d</sup>, D. Vilanova<sup>d</sup>,  
D. Wark<sup>k</sup>, A. Zghiche<sup>g</sup>, J. Zúñiga<sup>h</sup>.

The ANTARES Collaboration

- <sup>a</sup>*Centre de Physique des Particules de Marseille (CPPM), (CNRS/IN2P3 - Université de la Méditerranée Aix-Marseille II), 163 Avenue de Luminy, Case 907, 13288 Marseille Cedex 09, France*
- <sup>b</sup>*Centre de Physique Théorique (CPT), (CNRS), 163 Avenue de Luminy, Case 907, 13288 Marseille Cedex 09, France*
- <sup>c</sup>*Centre d'Océanologie de Marseille, (CNRS/INSU - Université de la Méditerranée), Station Marine d'Endoume-Luminy, Rue de la Batterie des Lions, 13007 Marseille, France*
- <sup>d</sup>*DAPNIA/DSM, CEA/Saclay, 91191 Gif Sur Yvette Cedex, France*
- <sup>e</sup>*Groupe de Recherches en Physique des Hautes Energies (GRPHE), (Université de Haute Alsace), 61 Rue Albert Camus, 68093 Mulhouse Cedex, France*
- <sup>f</sup>*IFREMER, Centre de Toulon/La Seyne Sur Mer, Port Bregailon, Chemin Jean-Marie Fritz, 83500 La Seyne Sur Mer, France IFREMER, Centre de Brest, 29280 Plouzané, France*
- <sup>g</sup>*Institut de Recherches Subatomiques (IReS), (CNRS/IN2P3 - Université Louis Pasteur), BP 28, 67037 Strasbourg Cedex 2, France*
- <sup>h</sup>*Instituto de Física Corpuscular (IFIC), CSIC - Universitat de València, 46100 Burjassot, Valencia, Spain*
- <sup>i</sup>*Laboratoire d'Astronomie Spatiale, Institut Gassendi pour la Recherche Astronomique en Provence (IGRAP), (CNRS/INSU - Université de Provence Aix-Marseille I), Les Trois Lucs, Traverse du Siphon, 13012 Marseille Cedex, France*
- <sup>j</sup>*Observatoire de Marseille, Institut Gassendi pour la Recherche Astronomique en Provence (IGRAP), (CNRS/INSU - Université de Provence Aix-Marseille I), 2 Place Le Verrier, 13248 Marseille Cedex 4, France*
- <sup>k</sup>*University of Oxford, Department of Physics, Nuclear and Astrophysics Laboratory, Keble Road, Oxford OX1 3RH, United Kingdom*
- <sup>l</sup>*University of Sheffield, Department of Physics and Astronomy, Sheffield S3 7RH, United Kingdom*

---

**Abstract**

The ANTARES collaboration has performed a series of *in situ* measurements to study the background light for a planned undersea neutrino telescope. Such background can be caused by  $^{40}\text{K}$  decays or by biological activity. We report on measurements at two sites in the Mediterranean Sea at depths of 2400 m and 2700 m, respectively. Three photomultiplier tubes were used to measure single counting rates and coincidence rates for pairs of tubes at various distances. The background rate is seen to consist of three components: a constant rate due to  $^{40}\text{K}$  decays, a continuum rate that varies on a time scale of several hours simultaneously over distances up to at least 40 m, and random bursts a few seconds long that are only correlated in time over distances of the order of a meter. A trigger requiring coincidences between nearby photomultiplier tubes should reduce the trigger rate for a neutrino telescope to a manageable level with only a small loss in efficiency.

*Key words:* Neutrino telescope, Sea water properties: luminescence, Undersea Cherenkov detectors.

*PACS:* 07.89.+b,13.15.+g,29.40.Ka,92.10.Bf,95.55.Vj

---

*Correspondence to:* N. Palanque-Delabrouille, DAPNIA/DSM, CEA/Saclay,  
91191 Gif Sur Yvette Cedex, France.  
Nathalie.Delabrouille@cea.fr

# 1 INTRODUCTION

The ANTARES<sup>1</sup> project [1] leads to the deployment of an undersea neutrino telescope (this concept was first proposed in [2]) with an area of 1/10 km<sup>2</sup> in a Mediterranean site 20 nautical miles off the coast from Toulon (France) at a depth of 2400 m. The location of the site is shown on figure 1. The ANTARES detector is aimed at the observation of neutrinos from astrophysical sources, an indirect detection of dark matter and the study of neutrino oscillations. An array of photomultiplier tubes detects the Cherenkov light emitted in the sea water from the muons produced by the neutrinos in the surrounding medium. At high energy, the muon is emitted in a direction close to that of the parent neutrino —  $\theta_{\nu\mu} \simeq 0.7^\circ/E^{0.6}(TeV)$  — and its direction is derived from the arrival times of the Cherenkov light wave front on at least 5 optical modules (where each optical module contains a single photomultiplier tube). The detector will consist of about 1000 optical modules on several vertical strings read out via a single optical cable to shore.

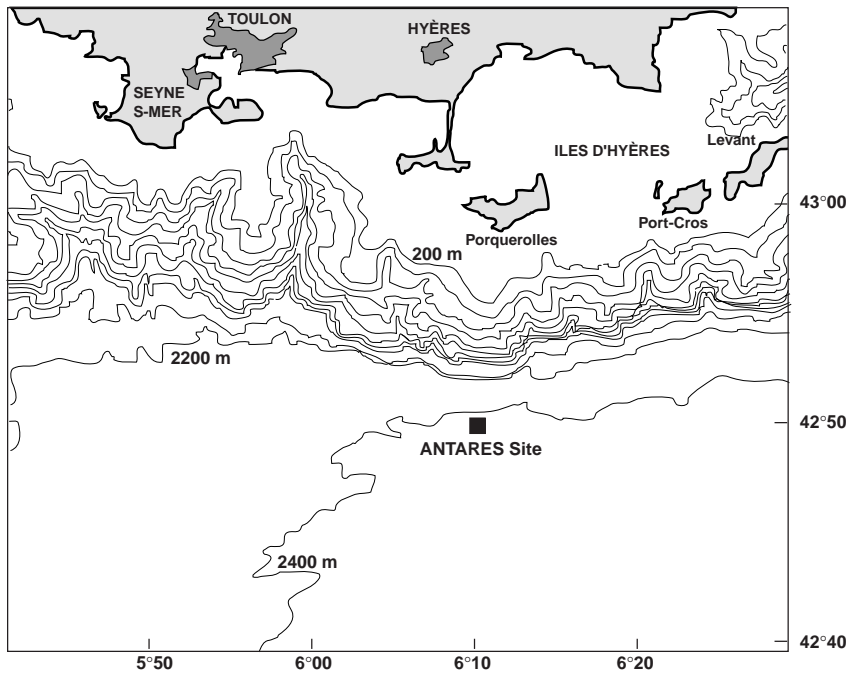


Fig. 1. Location of the ANTARES site, near the Mediterranean French coast.

As part of this project, we have developed measuring systems to characterize candidate detector sites for a proposed high energy neutrino facility. The selection criteria include the optical properties of the sea water, the depth of the site, its distance to the shore and the availability of technical support.

<sup>1</sup> Astronomy with a Neutrino Telescope and Abyss environmental REsearch.  
ANTARES WEB site: <http://antares.in2p3.fr/antares/antares.html>

Autonomous systems have been designed to measure *in situ* the background light, the fouling of glass spheres, and the light attenuation. Surveys with time ranges of the order of the year were carried out in order to study the seasonal variations of the sea properties.

Background light signals are expected from  $^{40}\text{K}$  decays<sup>2</sup> and possibly from biological activity. A knowledge of the background light behavior on site is of prime importance as it puts constraints on the trigger logic and electronics as well as on the mechanical layout of the optical modules. This paper reports on a series of tests dedicated to the measurement of this background which were performed on two sites in the Mediterranean sea.

## 2 DESCRIPTION OF THE MEASUREMENT

### 2.1 *Experimental set-up*

It is necessary to estimate how a detector will be affected by background light sources, through the measure of counting rates, coincidence rates, and their correlation at various distances. A set-up has been devised which can be used to study the time dependence of the background as well as its spatial extension and its correlation with undersea current. It was immersed for durations ranging from hours to months.

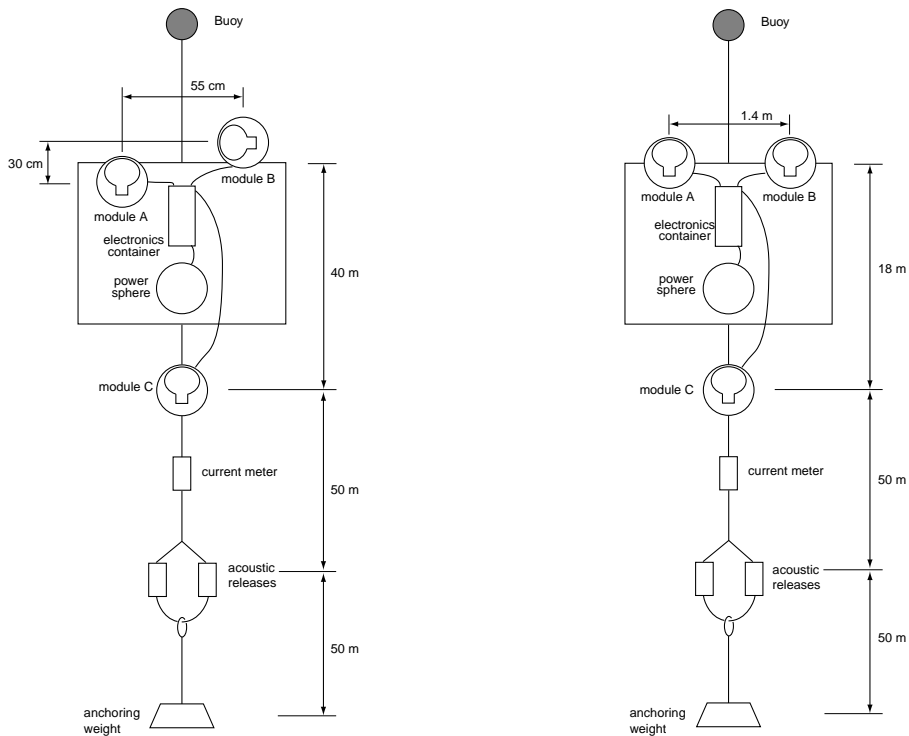
The measurements have been performed using optical modules with the same design as the ones which will be used for the final detector, except for the size of the phototubes (8" instead of 10" for the actual detector). Each optical module consists of a 17" pressure-resistant glass sphere housing an 8" Hamamatsu R5912 photomultiplier tube embedded in silicone gel to ensure a good optical coupling. A cage made from an alloy with a high magnetic permittivity surrounds each tube, shielding it from the terrestrial magnetic field. To monitor the efficiency of the photomultiplier tube, an alpha source was placed in each optical module.

The optical modules were deployed on "mooring lines" in the two configurations shown in figure 2. Our standard mooring line has (as indicated in figure 2 from bottom to top) an anchoring weight (iron chains, about 300 kg) followed by a pair of releases controlled remotely via an acoustic transducer and mounted in parallel for redundancy, and a current meter to measure the velocity of the water past the line. Buoys placed at the top of the line keep it taut and vertical. An Argos beacon and a flasher beacon assist in locating

---

<sup>2</sup>  $^{40}\text{K}$  undergoes  $\beta$ -decay (89.3%) and electron capture (10.7%).

the line after release, during recovery. For the measurement described here, a rigid frame is incorporated into the mooring line, holding two optical modules (“A” and “B”), an anodized aluminum cylinder housing the electronics and the data acquisition system, and a “power” sphere holding batteries. A third optical module “C” (not present in all tests) is attached to the mooring line, below this frame. The orientation of the optical modules and the distances between them were varied as shown in figure 2.



(a) Line for data sets 1 and 2.

(b) Line for data set 3.

Fig. 2. The two configurations of the mooring lines immersed for the measure of the contribution from background light. Elements are not to scale.

## 2.2 Data acquisition

The electronics and data acquisition system required for our stand-alone tests have been developed around a MBX 9000 acquisition card from MII (Micro Informatique pour l’Industrie), equipped with two Mbytes of RAM for data storage [3]. Digital and analogue I/O’s including two serial links are available for communication with each specific piece of equipment such as current-meter, acoustic modem and the MBX extension card that holds the electronics needed

for each test. A Unix-like real-time operating system runs on the processor. A configuration file describing the test sequence is read by the acquisition program at the startup of the processor. Single rates as well as prompt and delayed coincidences are counted for two detectors (either A and B, or A and C) on four 100 MHz scalars. The recorded data comprises:

- the time needed to reach a preset count on the singles scaler for module A,
- the counts reached during this period on the B/C singles scaler,
- the coincidence counts (with a 100 ns time gate width) on the AB/AC coincidence scaler,
- the random coincidence counts with B/C obtained, on the fourth scaler, by delaying the signals from detector A.

With deadtimes not exceeding  $1 \mu\text{s}$ , this technique gives sensitivity to frequencies up to a few MHz. Parameters such as tilt, current speed, direction of the Earth's magnetic field, temperature, depth and salinity are monitored during the entire detector operation.

### 2.3 Data sets

The analysis of three sets of data is presented.

**Set 1** was taken 20 nautical miles off Toulon ( $42^{\circ}50'$  N,  $6^{\circ}10'$  E, called hereafter the "ANTARES site") at a depth of 2430 m, measured at the level of the acoustic releases, with the configuration shown in figure 2a. Twelve hours of data were collected during the night of October 7-8, 1997.

**Set 2** was taken with the same configuration but at a site 20 nautical miles off Porto, Corsica ( $42^{\circ}22'$  N,  $8^{\circ}15'$  E) at a depth of 2680 m. Data were collected during a 20 minute period, three days a week, from October 10, 1997 to February 12, 1998.

**Set 3** was taken at the ANTARES site at a depth of 2430 m using the configuration of figure 2b. Data were collected for 4 hours, three days a week from March 10, 1998 to April 8, 1998.

The counting rates were measured successively at two different amplitude thresholds corresponding to 0.3 and 2 times the average photoelectron pulse height. The set-up used allows the study of correlations between signals at distances of 55 cm, 1.4 m, 18 m and 40 m, as well as their dependence on current velocity.

### 3 ANALYSIS

The data acquired as above were converted into counting rates as a function of time for each of the optical modules. A typical time stream is shown in figure 3, along with the distribution of the counting rates.

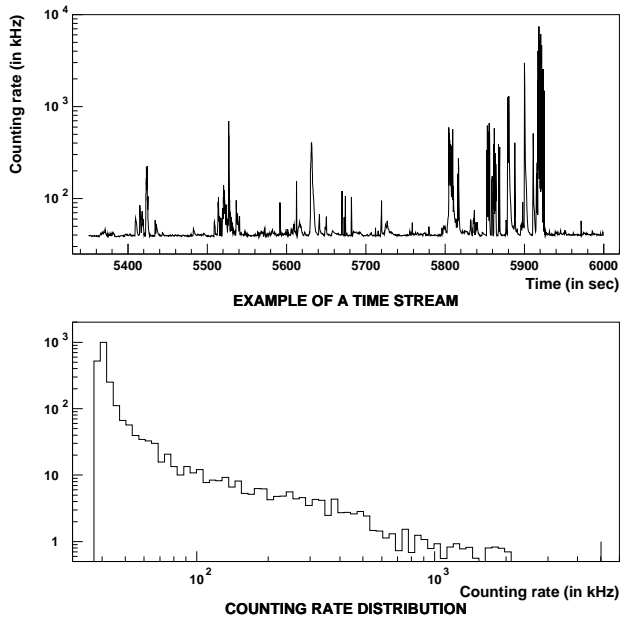


Fig. 3. Top panel: typical time dependence of the counting rate at the 0.3 photoelectron level (from set 1). Bottom panel: distribution of the counting rates for the above time stream. There is a sharp cutoff at a rate of  $\sim 35$  kHz, corresponding to the level of the background light continuum. The high frequency component of the spectrum corresponds to activity in the burst regime.

As can be seen in figure 3, the data stream consists of two components: a continuum base rate of a few tens of kHz, varying slowly on time-scales of a few hours, and sharp peaks lasting a few seconds and rising to tens of MHz (“bursts”). These two contributions will be studied separately.

#### 3.1 Background light — continuous component

The continuous component of the background light is defined as the lower envelope of the distribution of the counting rate of a given optical module as a function of time. The activity fluctuates by as much as 14 kHz on a time scale of a few hours (see table 1 and figures 6 and 8, top panels). This level varies simultaneously on all optical modules even when located 40 m apart.

No correlation is observed between this modulation and the current velocity.

Table 1

Variation of the level of the continuous component of the background light. The impact of fouling is negligible compared to the modulation amplitude.

<i>Set</i>	<i>Time of year</i>	<i>Location</i>	<i>Background (in kHz)</i>	
			<i>Minimum</i>	<i>Maximum</i>
1	Oct. 97	ANTARES site	37	47
2	Oct. 97 - Feb. 98	Corsica	24	27
3	Mar. 98 - Apr. 98	ANTARES site	20	34

A fraction of this continuous component is expected to be caused by the radioactive decay of potassium. The water salinity (38.5 ‰) is constant in time and the same at both sites, so the  $^{40}\text{K}$  contribution must also be constant in time, unless the water transparency fluctuates by a large amount. We therefore estimate an upper limit on the  $^{40}\text{K}$  contribution as the lowest measured rate: 20 kHz.

The modulation in the continuum is probably caused by a variable bioluminescence component. The amplitude of the modulation is larger in the ANTARES site than in Corsica, which hints at a higher activity of the continuous luminescence background, although we cannot exclude seasonal effects or any long-period variation.

Setting the threshold to 2 photoelectrons suppresses the background counting rate by about a factor of 100, reducing it to  $\sim 300$  Hz, with a contribution of  $\sim 150$  Hz from the  $^{40}\text{K}$  contained in the glass sphere and from the emission of the  $\alpha$  sources located in each of the optical modules (used to monitor the PMT efficiency).

The 2 photoelectron background is well correlated with the 0.3 photoelectron background in the sense that it exhibits a coherent modulation with the same relative amplitude as the 0.3 photoelectron signal. This suggests that most of the remaining 2 photoelectron background comes from the tail of the 1 photoelectron distribution.

### 3.2 Background light — burst regime

Short bursts in the counting rate are observed, as shown in figure 3, probably due to the passage near the detector of light emitting organisms. The modulation of the continuous component is not correlated with periods of high burst activity, so the two effects are probably caused by distinct populations. This is observed in each of the three data sets.

The burst rate may be defined as the fraction of time a given optical module exhibits a counting frequency above 200 kHz at the 0.3 photoelectron level. This threshold is chosen because the data acquisition system is expected to suffer significant deadtime above 200 kHz. The mean values (i.e. averaged over the entire test period) of the rates  $R_A$ ,  $R_B$  and  $R_C$  (for modules A, B and C respectively) are given in table 2. The rates  $R_{AB}$  and  $R_{AC}$  are defined as the fraction of time that the two modules A and B or A and C are simultaneously exhibiting singles counting rates above 200 kHz.

Table 2

Fraction of time a given optical module is affected by bursts (see definition in text). The values for 18 m are derived from a single sequence of data and thus affected by a larger uncertainty. Separations of 0.55 and 1.4 m are obtained with modules A and B, while separations of 18 and 40 m are with modules A and C.

<i>Set — Location</i>	<i>Distance AB/AC</i>	<i>Time of year</i>	$R_A$	$R_{B/C}$	$R_{AB/AC}$
1 - ANTARES site	0.55 m	Fall	4.8%	6.2%	4.4%
1 - ANTARES site	40 m	Fall	4.6%	6.0%	< 0.1%
2 - Corsica	0.55 m	Fall	1.2%	3.1%	1.0%
3 - ANTARES site	1.4 m	Spring	1.6%	1.5%	1.0%
3 - ANTARES site	18 m	Spring	2.1%	1.3%	< 0.1%

For data sets 1 and 2,  $R_B$  is systematically higher than  $R_A$  (A and B are the two “close” modules), which can be understood by the different orientation of these two modules: A is looking up while B is looking towards the horizontal (cf. figure 2). As mentioned below, the bursts are correlated with the current (an horizontal westwards stream, in the ANTARES site) which therefore could influence differently the burst rates on modules A and B. This is corroborated by the fact that in set 3 both modules face the zenith and detect the same burst rate.

There is a clear indication for correlation between the periods of burst activity for two modules located near one another, whereas this correlation is negligible for distant modules: two optical modules within 1.4 m of each other detect bursts simultaneously, while two modules located 40 m apart are affected at random uncorrelated times (rate for both being affected simultaneously smaller than 0.1%). Two modules 18 m apart also seem to be affected at random uncorrelated times, but additional data are required to assess this result with more confidence. An example of time streams and their burst correlation is illustrated in figure 4.

The dependence of burst activity on current velocity is emphasized in figure 5. A strong correlation between the two variables is observed. However, the results from the three data sets differ significantly. It is natural to interpret

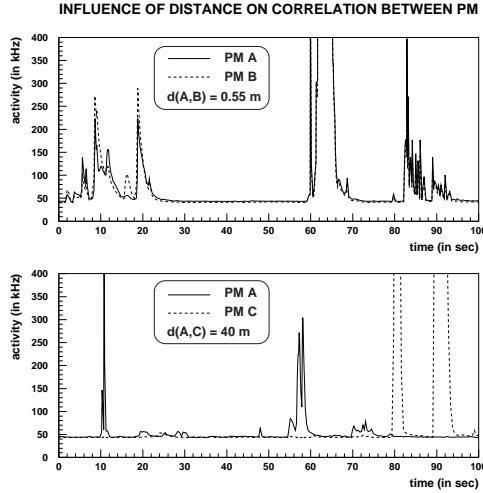


Fig. 4. Example of time streams illustrating the strong correlation between the counting frequencies of modules located 0.55 m apart and the negligible correlation for modules 40 m apart (data from set 1).

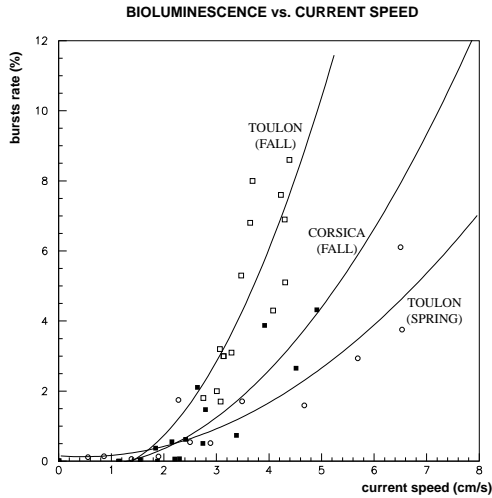


Fig. 5. Correlation between the burst rate ( $R_{AB}$  as defined in the text) and the current velocity, for all three tests. A fit with a second degree polynomial is superimposed on top of the data from each individual test.

this as reflecting a dependence on site and season, but more data would be required to confirm such an interpretation. During the test off Corsica, the current speed was on average smaller than in Toulon and a lower burst activity was observed. This statement needs to be validated on a longer time scale.

These data show that bursts are a local phenomenon affecting a given optical module at most  $\sim 6\%$  of the time. A seasonal dependence might explain the fact that this value is down to  $\sim 2\%$  in set 3.

### 3.3 Coincidences between optical modules

#### 3.3.1 Coincidence rates

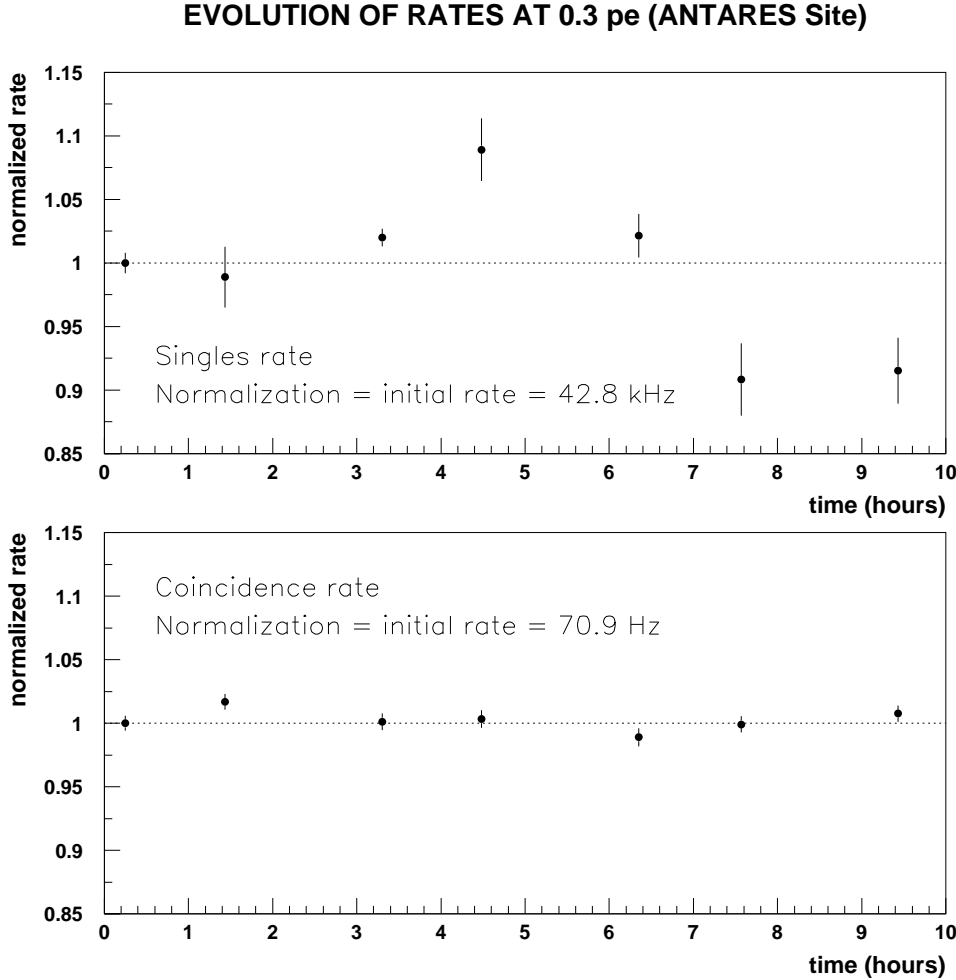


Fig. 6. Evolution with time of the singles rate continuous component (top panel) and the coincidence rate (bottom panel) between modules A and B, in the ANTARES site (data set 1). Both rates are normalized to their initial value.

Figure 6 illustrates the evolution with time of the coincidence rates between modules A and B measured at the 0.3 photoelectron level with a 100 ns time window, for data set 1, where periods of bursts have been cut out. The variation of the singles rate over a 12 hour period (top panel) is simply the variation of the continuous component as discussed in section 3.1. In contrast, the coincidence rate is constant over the same period. This indicates that coincidences are produced by the  $^{40}\text{K}$  decays, which occur at a constant rate, and not by the variable component (presumably bioluminescence) of the continuous contribution.

The coincidence rates, corrected for accidentals by subtracting from the measured rate the delayed coincidence rate, are summarized in table 3 (“Coincident rate”). The contribution to this rate from the  $\alpha$  source contained in each optical module (see figure 7) was measured in air and is also indicated in the table. The correction applied is affected by a systematic uncertainty due to the different media (air vs. water). The reduced coincidence rates, after subtraction of the  $\alpha$  source contribution, are given in the last column (“Reduced rate”). We observe a null coincidence rate at the 2 photoelectron level.

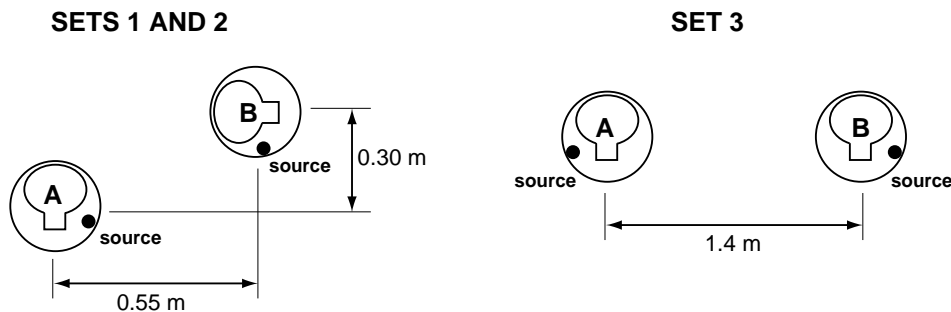


Fig. 7. Position of the  $\alpha$  sources in the glass spheres.

Table 3

Coincidence rates for all three tests (see text for details).

<i>Set</i>	<i>Threshold (in pe)</i>	<i>Coincident rate (in Hz)</i>	<i><math>\alpha</math> sources (in Hz)</i>	<i>Reduced rate (in Hz)</i>
1	0.3	71	52	19
1	2.0	15	17	$\sim 0$
2	0.3	71	52	19
3	0.3	11	$\sim 0$	11
3	2.0	0	$\sim 0$	0

The coincidence rate from  $^{40}\text{K}$  is thus 19 Hz at the 0.3 pe level for two modules located 55 cm apart, whether near Toulon or near Corsica, and down to 11 Hz at the 0.3 pe level for two modules located 1.4 m apart, for the geometries shown in figure 7. The continuum background noise can thus be suppressed by three orders of magnitude by requiring coincidences, as compared to the singles rate (see section 3.1). At the 2 pe level, the coincidence rate vanishes.

### 3.3.2 Comparison with a Monte Carlo calculation

An estimate of the counting rates due to  $^{40}\text{K}$  was obtained using a Monte Carlo simulation based on GEANT 3.21 [4]. A  $^{40}\text{K}$  activity of 13 Bq per liter and an effective attenuation length of 41 m (as measured at the same site in December 1997 [5]) were assumed (the counting rate is directly proportional

to the effective attenuation length). All the components of the optical module were taken into account (in terms of efficiency or shielding).

The simulation yields the following rates at the 0.3 photoelectron threshold:

singles rate:		18 ± 3 kHz
coincidence rates:	Sets 1 & 2	28 ± 4 Hz
	Set 3	11 ± 3 Hz

Given the uncertainty on the  $\alpha$  source correction, these numbers are in good agreement with the observations described previously. As observed in the data, the simulation gives negligible coincidence rates at the 2 photoelectron threshold (less than 1 Hz).

### 3.3.3 Effect of fouling

The decrease of the coincidence rate with time is due to fouling on the modules (cf figure 8, bottom panel), whether due to sedimentation or to the growth of bacteria on the surfaces. It is mostly noticeable on the evolution of the coincidence rate since the evolution of the singles rate is dominated by the large modulation of the background light continuum. On a large time scale however, as for the test in Corsica, both singles and coincidence rates decrease in a similar fashion (figure 8). No effect is noticeable in the first test on the ANTARES site, which only lasted 12 hours (figure 6, bottom panel).

The global effect of fouling can be estimated from the decrease in the coincidence rates observed in sets 2 (120 days near Corsica) and 3 (30 days near Toulon), taking into account the presence of the  $\alpha$  sources (see figure 7). Let  $t_A$  and  $t_B$  be the local transmission efficiencies near the  $\alpha$  sources of modules A and B (for the light emitting module),  $\langle t \rangle$  be the transmission efficiency averaged over the optical module (for the light receiving module),  $f$  the coincidence rate detected,  $f_\alpha$  the rate of the  $\alpha$  sources (subscripted by A and B in the following equation for the sake of clarity, but assumed to be equal) and  $f_{40K}$  the coincidence rate generated by the  $^{40}\text{K}$  background. In general, we can write

$$f = \langle t_A \rangle \langle t_B \rangle f_{40K} + \langle t_A \rangle t_B f_{\alpha, B} + \langle t_B \rangle t_A f_{\alpha, A} \quad (1)$$

In the second and third terms of the right-hand side of this equation, the  $\langle t \rangle$  coefficients should be affected by a second-order correction since regions of the detector facing the  $\alpha$  source contained in the other sphere are actually favored. This effect is not taken into account.

### EVOLUTION OF RATES AT 0.3 pe (Corsica)

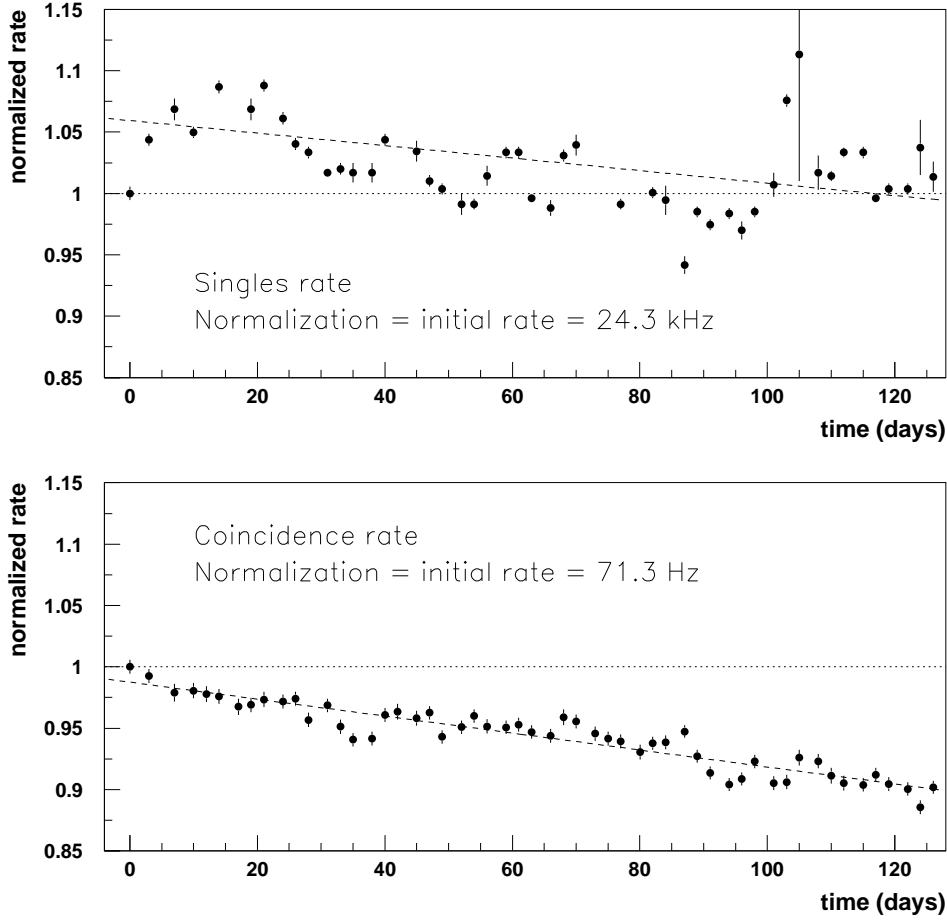


Fig. 8. Evolution with time of the singles rate continuous component (top panel), and the coincidence rate (bottom panel) between modules A and B, in Corsica (data set 2). Both rates are normalized to their initial value.

Equation 1 can be simplified and solved to first order for the most significantly affected module(s). An extensive study of the effect of fouling has been performed by the ANTARES collaboration with a dedicated set-up [6], showing that most fouling is for surfaces pointing directly at the zenith, decreasing quickly with angle. The local transmission efficiencies  $t_A$  and  $t_B$  are thus assumed to be constant since the  $\alpha$  sources are located below the equator of the glass sphere. The contributions from  $^{40}\text{K}$  and the  $\alpha$  sources are also assumed constant. For set 2,  $\langle t_B \rangle$  is assumed constant since the module is pointing at  $90^\circ$  with the respect to the zenith, while in set 3, we consider that  $\langle t_A \rangle = \langle t_B \rangle$  (both facing the zenith). The effect of fouling on a module in the ANTARES site is then estimated to be:

$$\langle t \rangle_{(\theta=0^\circ, \Delta t=30 \text{ days})} = 76\% \quad (2)$$

where  $\theta$  is the angle between the axis of the module and the zenith and  $\Delta t$  the duration of the experiment. For the test immersed in Corsica, we measure:

$$\langle t \rangle_{(\theta=0^\circ, \Delta t=120 \text{ days})} = 87\% \quad (3)$$

The Corsica site, in fall, thus seems cleaner than that near Toulon. It could, however, be only a seasonal fluctuation.

Significant residual fluctuations can be observed around the average decrease of the coincidence rate (see plot of figure 8, bottom panel). They are probably caused by a non-constant fouling rate, due for instance to the temporary “cleaning” effect of current. On a 30 day period, these fluctuations can induce an uncertainty on the rate of fouling which can account for the difference in the estimates obtained in equations 2 and 3.

## 4 DESIGN CONSTRAINTS

The ANTARES collaboration proposes to build a first detector consisting of 1000 optical modules housing 10'' photomultiplier tubes (instead of the 8'' tubes used for the measurements presented in this paper — singles rates given in this article have therefore been scaled by 1.6 for the following estimates), leading to an effective area of 0.1 km<sup>2</sup>. We here infer the constraints put on the design of an undersea neutrino telescope from the measured characteristics of the background light.

### 4.1 Trigger and electronics

In order to cope with the background light and the fouling, we plan to arrange optical modules in clusters of 3 optical modules facing away from each other with their axis making an angle of 45° with the vertical, and to use twofold local coincidences in the trigger. This reduces the accidental rate per cluster to a few 100 Hz. The rate due to <sup>40</sup>K coincidences in the planned configuration is negligible. A majority trigger condition for the whole detector is built from these coincidences. Requiring four coincidences yields a trigger rate of a few kHz, provided that clusters affected by bursts of bioluminescence are inhibited.

An analogue memory in an ASIC has been designed in which the photomultiplier pulses and arrival times can be stored. The memory depth is sufficient to cover the time needed for the trigger to be built and a read-out request to be sent back to the whole array [7]. Given the size of the detector, this time comes mostly from the propagation of signals to and from the central

node ( $10 \mu\text{s}$ ). If a request is received during a time window constrained by the trigger causality, the data are digitized and sent to the shore station. They are otherwise discarded.

The deadtime induced by the counting rate will be negligible up to several 100 kHz. When integrated over the distribution shown in figure 3 (bottom) and the spatial distribution inferred from table 2, the overall effect of this deadtime is less than a 5% inefficiency distributed randomly over the detector.

#### *4.2 Muon track determination*

The background light has two effects : below the maximum rate which can be handled by the electronics, it results in spurious hits added to those coming from the muon track; above this rate it will temporarily blind parts of the detector, as mentioned above. These blind spots can be located as a function of time, and their effect on the acceptance inferred, by monitoring the counting rate of all optical modules.

Monte Carlo studies show that for a majority trigger requiring at least four coincidences, each event contains about ten additional single photomultiplier tube hits coming from the Cherenkov light emitted by the muon.

A 50 kHz background counting rate produces about 100 isolated noise hits randomly distributed over the entire volume, during the  $2 \mu\text{s}$  muon time of flight. A first-try track fit is obtained by fitting a straight line through the hits on coincident optical module pairs. Limiting the useful volume to a 50 m radius cylinder around this initial track, and the time difference with respect to this preliminary fit prediction to 200 ns, only 1 noise hit remains on average. This causes a negligible distortion to the calculated muon direction.

## **5 CONCLUSION**

The counting rates due to background light have been measured at two different sites. It is composed mainly of three independent components: a constant rate due to the beta decay of  $^{40}\text{K}$  naturally present in the sea salt, another slowly fluctuating on time scales of a few hours, and one exhibiting bursts a few seconds long, probably due to the luminescence of living organisms.

We observed a strong correlation between the undersea current velocity and the bursts, although the absolute dependence seems to be affected by seasonal variations. While the bursts occur simultaneously for two optical modules located less than 1.4 m apart, they are uncorrelated for modules located more

than 40 m apart. The modulation of the continuous component, however, is correlated on at least a 40 m range.

Measured coincidence rates are in agreement with a Monte Carlo simulation of the Cherenkov light caused by the beta decay of  $^{40}\text{K}$ . Long term decreases of these coincidence rates are compatible with independent measurements of optical fouling.

The background light has only a minor effect on the performance of an undersea neutrino telescope. An electronics system is being developed which can handle rates up to several 100 kHz without significant deadtime. A tight timing window reduces background hits to a rate that does not affect the determination of the muon direction and energy.

## References

- [1] ANTARES proposal, <http://antares.in2p3.fr/antares/proposal99.html>.
- [2] Markov, M.A., in Proc. of Annual International Conference of High Energy Physics, Rochester (1960).
- [3] Gournay, J.F. et al., ICALEPCS 97 proceedings, Beijing (1997).
- [4] Geant3.21 manual, [http://wwwinfo.cern.ch/asdoc/geant\\_html3/geantall.html](http://wwwinfo.cern.ch/asdoc/geant_html3/geantall.html), PHYS325.
- [5] Palanque-Delabrouille, N., ICRC 99 proceedings, Salt Lake City (1999).
- [6] de Botton, N., ICRC 97 proceedings, Durban (1997).  
Palanque-Delabrouille, N., ICRC 99 proceedings, Salt Lake City (1999).
- [7] Lachartre, D., Beaune 99 proceedings, Beaune (1999).